Experiments in a Representative Environment

Gilles Pijaudier-Cabot, Christian La Borderie, Thierry Reess, Wen Chen, Olivier Maurel, Franck Rey-Bethbeder, Antoine Silvestre de Ferron

Experiments in a Representative Environment

Gilles Pijaudier-Cabot, Christian La Borderie,
Thierry Reess, Wen Chen, Olivier Maurel,
Franck Rey-Berbeder and Antoine de Ferron

The experimental program presented in this chapter included several distinct phases:

– mechanical experiments in which specimens were subjected to representative confinement stresses and to pulsed arc electrohydraulic discharges (PAEDs);

– permeability tests performed before and after the mechanical experiments in order to quantify the increase in permeability upon electrohydraulic fracturing;

– X-ray scanning tomography before and after the mechanical experiments in order to visualize the crack network generated by the mechanical loads.

We are going to detail the experiments and discuss the results obtained on a model material (mortar), and on sandstone.

1.1. Mechanical set-up

Our aim is to design experiments that implement conditions that are that are as close as possible to real ones.

It means that specimens ought to be subjected to the triaxial confinement experienced underground at several different depths, and that the pulse applied should be generated in a specimen geometry that is close to a real well bore.

The shock wave is generated in a hollow cylinder (mortar or rock) filled with water. The radial confinement pressure is applied with three stacked steel rings (600 mm in diameter, 60 mm in height and 30 mm thick) tightened with the help of a beam wrench. The steel rings were equipped with strain gauges to check the confining pressure during the tightening phase. Three confining blocks made of ultra high-performance concrete reinforced with metallic fibers are placed between the specimen and the steel rings in order to absorb the shock wave and to homogenize the radial pressure on the external face of the specimen. The high-performance concrete used to confine the specimen has approximately the same dynamic impedance characteristics as the specimen in order to avoid wave reflections at the boundary. This set-up is shown in Figure 1.1.

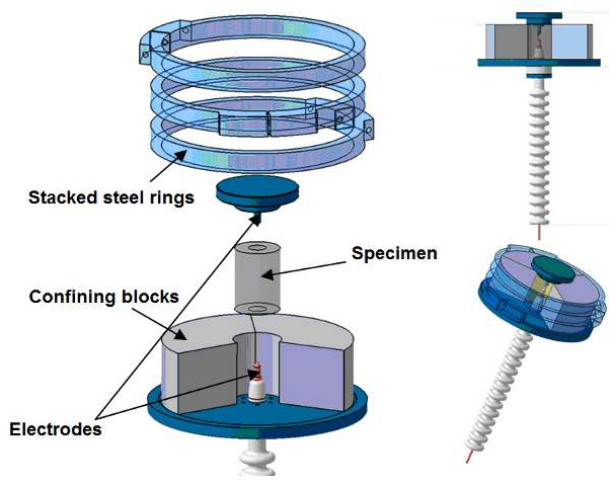

Figure 1.1. *Overall view of the triaxial cell*

The vertical load is applied with a 2,000 kN hydraulic jack (Figure 1.2), which is placed in a protected environment with respect to electromagnetic radiations and electrical surges.

Figure 1.2. *Hydraulic frame hosting the triaxial cell*

Due to the radiations generated by the electrical discharges, it was not possible to use the displaced transducers or electronic equipment for load control or resistive gauge measurements. For this reason, the frame is a pneumatic one, the confinement is applied in a passive way and no transducers were able to be placed in order to record loads or deformations.

Specimens are confined according to three levels of radial stresses and vertical loads corresponding to three depths: low confinement (depth = 0 m), medium confinement (depth equal to 1,500 m and Biot factor equal to 1) and high confinement (depth equal to 2,250 m and Biot factor equal to 0.5 or depth equal to 3,000 m and Biot factor equal to 1). Vertical and lateral stresses are detailed in Table 1.1.

	Vertical loads (MPa)	Lateral stresses (MPa)	Depth (m)
Low confinement	2	2	0
Medium confinement	19.5	9.1	1,500
High confinement	40	25	2,250

Table 1.1. *Vertical and lateral stresses of the mortar*

1.2. Pulsed arc electric generator

The electrodes are placed inside the hollow part of the specimen which is immersed in water (Figure I.1). The electrodes are made up of two vertical cylindrical tubes, on the lower ends of which are screwed two stainless steel electrodes (5 mm diameter). The gap between the two electrodes is equal to 5 mm. The positive impulse voltage is obtained by charging storage capacitors in the C = 300 nF to 21 μF range, depending on the electrical energy to be released during the electric discharge. A triggered spark-gap allows the switching of energy of up to 20 kJ in water. The maximum charging voltage of the capacitors is 40 kV. The voltage impulse and the current are monitored with a North Star probe (100 kV–90 MHz) and a Pearson current monitor (50 kA–4 MHz), respectively.

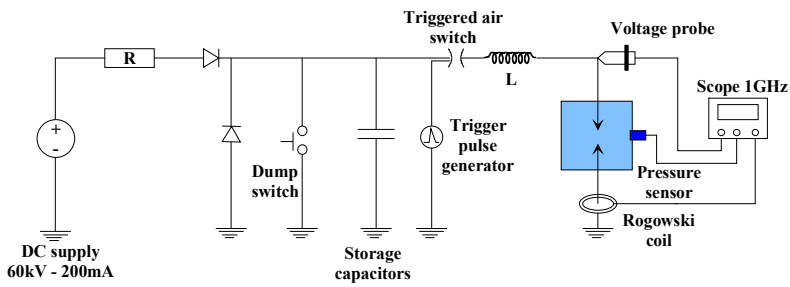

Figure 1.3. *Experimental set-up – electrical part*

Figure 1.3 shows the schematic organization of the electrical set-up. During the tests, the pressure sensor is removed. It is used for the calibration of the energy–pressure relationship only. According to previous investigations [TOU 06], the dynamic pressures generated by subsonic water discharges present in bi-exponential form and are characterized by a rise time of about 500 ns and a pulse width of a few microseconds. The associated frequency spectrum reaches 200 kHz at –20 dB.

The general form of the pressure pulse applied can be written using the following relationship:

$$P(t) = P_0\left[e^{-at} - e^{-bt}\right] \qquad [1.1]$$

where P is the pressure at time t, P_0 denotes the peak pressure value and a and b are the constants in our experimental conditions. Previous works [TOU 06] have pointed out that the peak pressure P_0 the depends on the energy E_B remaining at breakdown time (point at which liquid water in between the electrodes breaks down) and can be approximated by:

$$P_0 = \frac{k}{d}\left(\frac{E_B}{E}\right)^{\alpha} \qquad [1.2]$$

where $E_B = 1/2.C.U_B^2$. U_B is the breakdown voltage value, C is the storage capacity, k, α and E are the parameters that depend on the interelectrode geometry and d is the distance between the specimen and the plasma channel. In the same experimental conditions (where the distance between the electrodes is 5 mm, and the radius of the electrodes is 15 mm), Touya has shown that $\alpha = 0.35$ and $k = 9000/d$. Thus, it is possible to control the peak pressure value P_0 applied to mortar specimens using the following relation:

$$P_0 = \frac{9000}{d}.E_B^{0.35} \qquad [1.3]$$

with P_0 in bar, E_B in kJ and d in mm. Consequently, the applied peak pressure can be adjusted by changing the value of the remaining energy E_B or by modifying the charging voltage and capacity.

1.3 Material properties

The specimens are hollow cylinders with internal diameter, external diameter and height equal to 50, 125, and 180 mm, respectively, as shown in Figure 1.4. Two materials have been considered: mortar and sandstone.

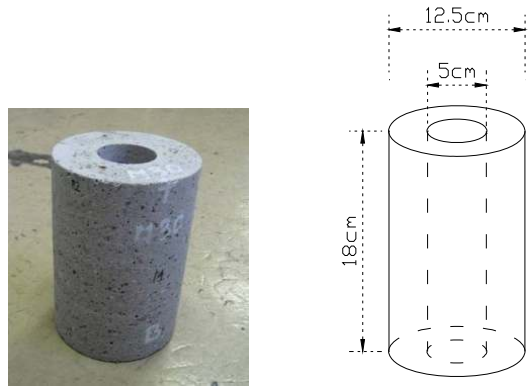

Figure 1.4. *Specimen characteristics*

For the cement-based specimens, mortar was made with a maximal grain size of 2 mm and with a water-to-cement ratio equal to 0.6. It is a model material designed in such a way that its initial permeability is close to that of tight rocks. The properties of this mortar are given in Table 1.2. Sandstone specimens were machined to the same geometry as mortar ones. Mortar specimens are machined too in order to avoid the effects of segregation that naturally exist at the mould boundaries.

	f_c (MPa)	f_t (MPa)	E (MPa)	K_v (m^2)
Mortar	19.6	4.9	17,300	$4.\ 10^{-17}$
Molière sandstone	49	6.35	19,000	1.10^{-17} to 2.10^{-16}

Table 1.2. *Average mechanical properties of mortar and sandstone*

1.4. Measurements of radial permeability

Radial permeability tests are performed in isothermal (ambient) conditions. An inert gas (nitrogen) is injected into the cylindrical borehole through a perforated bottom platen and flows radially through the specimen (Figure 1.5). In order to achieve radial flow of the gas, the top and bottom faces of the cylindrical specimen are covered with an aluminum foil and with silicone grease in order to prevent leakage. In addition, the platens placed on the upper and lower faces have two cylindrical rubber joints. The measurement of the intrinsic permeability of mortar is performed at 20°C, under an axial compressive load of 4 kN, resulting in the compressive stress of 0.4 MPa, a negligible stress for such a specimen. This load ensures contact between the specimen and the load platens, and therefore the tightness of the permeability cell. A relative pressure ΔP (difference between the injection pressure P_i and the atmospheric pressure P_{atm}) is applied and maintained until gas flow is stationary. The relative pressure and mass flow rate are measured upstream of the specimen with a set of mass flow meters that converts the mass flow rate into an equivalent volumetric gas flow rate. Each flow meter has a different range, starting from 10–150 ml/min, via 50–1,500 ml/min, to 300–15,000 ml/min, allowing us to scan intrinsic permeabilities from $10^{-18}$to 10^{-10} m^2.

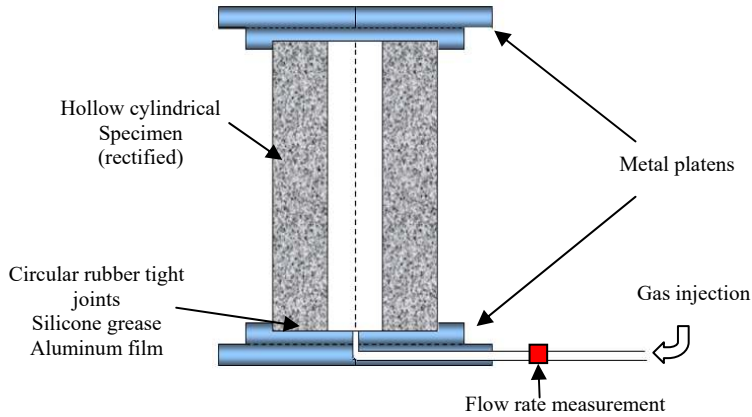

Figure 1.5. *Schematic representation of the permeability cell*

Darcy's law and mass balance equation enable an apparent permeability K_a [m²] to be calculated from the injection flow rate Q_i [m³/s]:

$$k_a = \frac{Q_i \cdot P_i \cdot \mu \cdot \ln\left(\frac{r2}{r1}\right)}{\pi \cdot h \cdot \left(P_i^2 - P_{atm}^2\right)} \qquad [1.4]$$

where μ [Pa.s] is the dynamic viscosity of the inert gas used (nitrogen) and r_1 [m], r_2 [m], and h [m] are the inner radius, outer radius and the height of the cylindrical specimen, respectively.

This permeability is relative to the overall gas flow through the material, consisting of the viscous flow and the slip flow. Viscous flow corresponds to the classical laminar configuration. The slip flow appears when the average diameter of the pores is the size of the mean free path of the gas molecules (average distance between collisions). In

this case, there is an interaction between the gas and the pore walls that cannot be neglected.

In order to obtain the intrinsic permeability related to viscous laminar flow, a characteristic of the sole porous medium, the relationship due to the Klinkenberg model is used, as in the experiments reported in the introduction (equation [I.1]). The intrinsic permeability K [m^2] is obtained by extrapolating the apparent gas permeability measured at various pressures to the case of infinite pressure. The measurements of the apparent permeability are performed for five relative pressures: 0.3, 0.25, 0.20, 0.15 and 0.10 MPa. The accuracy of measurement of the apparent permeability is approximately 2%. The permeability is measured on each specimen prior to mechanical testing and serves as a reference value in forthcoming comparisons.

The permeability after mechanical testing was measured without confinement stresses and also checked on representative specimens with confinement stresses applied. As expected, the permeability measured under confinement was lower than the one measured without confinement. The ratio between permeability measured under medium confinement and without confinement is approximately equal to one order of magnitude. We will see that the variation of permeability due to electrohydraulic fracturing is much larger than that.

1.5. X-ray tomography

Each specimen was scanned in an X-ray tomography facility prior to and after testing. The specimens were marked so that the three-dimensional (3D) images could be superimposed and then relative permanent displacements between the two images could be recovered. These residual displacements are due to cracks that stay open after testing. The technique is such that residual crack opening of a few

tenths of a micron can be obtained from images with an accuracy of 250 µm corresponding to a medical X-ray tomographic device.

1.6. Results on model materials

Two sequences of tests have been carried out. In the first one, the mortar specimens were subjected to a single shock under a variable injected electrical energy, for each of the three confinement levels considered. For the tests under low confinement, the injected electrical energy ranges up to 680 J; for the tests under medium confinement, it ranged up to 1.15 kJ and the injected energy reached 17 kJ in the tests under high confinement.

In the second sequence, the specimens were subjected to repeated shocks (up to nine shocks) with a constant injected energy. Note that the time between each shock is in the order of several minutes in order to avoid any possible effects relating to fatigue.

1.6.1. *Influence of injected electrical energy on permeability*

The variation of intrinsic permeability of mortar specimens with injected electrical energy E_B at different confinement levels is shown in Figure 1.6.

If the injected electrical energy is below a threshold, the intrinsic permeability does not increase regardless of the level of confinement. This threshold increases with increased confinement. Permeability sharply increases with the injected energy.

When the permeability became greater than 1.00 10–14 m^2, it was not possible to measure it. Specimens were so damaged that macrocracks were observed throughout the thickness of the hollow cylinders, resulting in a very large

apparent permeability that could not be measured accurately with our equipment.

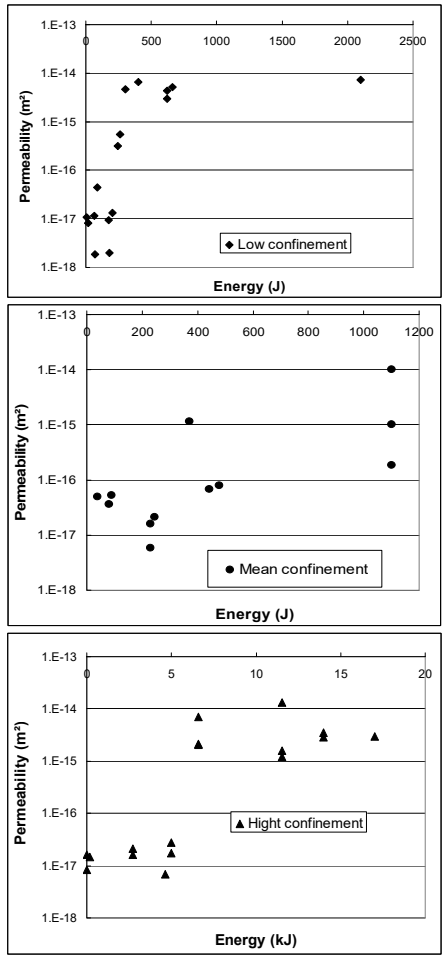

Figure 1.6. *Evolution of following a permeability with injected electrical energy, single shock on mortar specimens*

Under low confinement, a damage threshold of 190 J characterizes the onset of microcrack propagation. When the injected energy is below this threshold, microcracks do not

develop; when the injected energy is greater than this threshold, microcracks with an opening in the range of 0.02 mm are observed. This phenomenon will be illustrated with tomography X-Ray scans later. Under medium and high confinements, the same trend is observed, with different damaging energy thresholds of 500 J and 5.11 kJ, respectively.

1.6.2. *Influence of the number of shocks on permeability*

Tests with repeated shocks have been performed in the case of high confinement only.

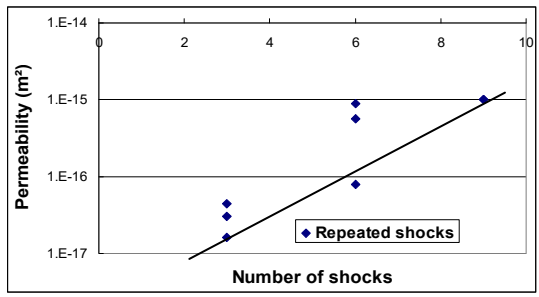

Figure 1.7. *Evolution of the permeability of mortar specimens with the number of shocks, under an injected energy equal to 2.7 kJ and high confinement*

The tests were carried out with two energy levels. The first level corresponded to 60% of the threshold of damage. Sixty and 90% shocks were applied. No significant changes in permeability were observed. This energy level was too low to damage the material significantly. The second energy level was at 85% of the threshold of damage. The number of shocks applied on each specimen ranged from 3 to 6 and 9 shocks.

The test results are shown in Figure 1.7. In a semi-log plot, the permeability increases almost linearly with the number of shocks. This increase spans over a range of almost two orders of magnitude, which is above the scattering of data.

1.6.3. *X-ray scans*

The correlations between the dynamic load applied on the specimens, their microstructure, material damage and the permeability can be visualized qualitatively with X-ray tomography. Figure 1.8 shows an example of the cross-section after scanning the specimen before and after shock, and the difference between the two scans. The level of gray varies linearly with the material density. White zones are related to pores and cracks. The resolution of the scan is approximately 0.25 mm. Taking the difference between the two scans provides an increase in resolution to about 0.02 mm. Large cracks with opening above 0.02 mm can be observed only. The darkest zones in the specimen represent the virgin material with density close to 2.5 kg/dm^3.

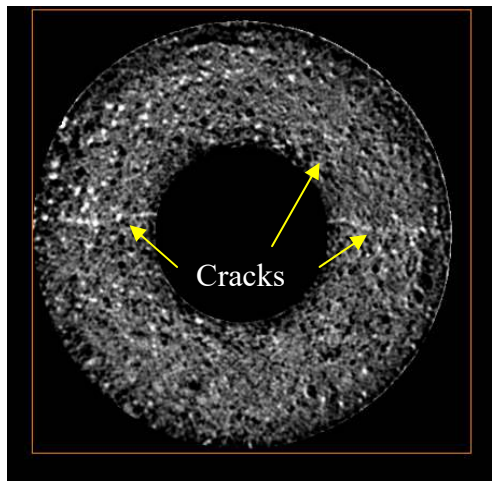

Figure 1.8. *Cross-section after computed tomography scanning of a mortar specimen*

Three-dimensional scans are shown in Figures 1.9 and 1.10. In these photos, the dark zones show macrocracks with an opening greater than 0.02 mm. Figure 1.9 shows the

effect of the level of electrical energy injected in the case of high confinement.

Quantitatively, the crack surface area generated may be used to analyze the effectiveness of the process. The specimens denoted as M08, T03 and M11 in Figure 1.9 had fracture surfaces of 63 cm^2, 439 cm^2 and 351 cm^2, respectively. This evolution correlates quite well with the specimens' evolution of permeability. Nevertheless, without a complete statistical analysis, which was not performed in the present study in view of the limited number of tests for each energy and confinement configuration, no robust quantitative correlation can be determined. Scans also show that several macrocracks had developed, which is at variance with a static (e.g. hydraulic-driven) process in which only a single macrocrack would propagate.

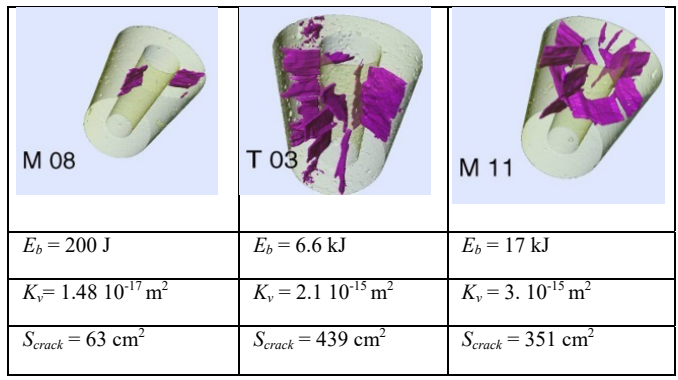

E_b = 200 J	E_b = 6.6 kJ	E_b = 17 kJ
K_v= 1.48 10^{-17} m^2	K_v = 2.1 10^{-15} m^2	K_v = 3. 10^{-15} m^2
S_{crack} = 63 cm^2	S_{crack} = 439 cm^2	S_{crack} = 351 cm^2

Figure 1.9. *Three-dimensional tomography scans after one shock under high confinement. For a color version of the figure, see www.iste.co.uk/pijaudier/drystone.zip*

Figure 1.10 shows the effect of the number of repeated shocks with injected electrical energy equal to 2.7 kJ on the generation of macrocracks under high confinement. After three shocks cracking slightly evolves, with a crack surface equal to 26 cm^2. Macrocracking occurs inside the specimen after six shocks, and the crack surface increases to

238.5 cm². After nine shocks, severe cracking is observed and the crack surface is increased to 326.5 cm².

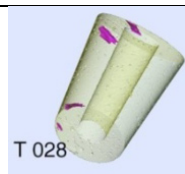	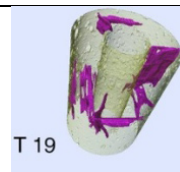	
E_b = 2.7 kJ	E_b = 2.7 kJ	E_b = 2.7 kJ
3 shocks	6 shocks	9 shocks
K_v= 3.01 10^{-17} m^2	K_v= 5.64 10^{-16} m^2	K_v = 1. 10^{-15} m^2
S_{crack} = 26 cm^2	S_{crack} = 238.5 cm^2	S_{crack} = 326.5 cm^2

Figure 1.10. *Three-dimensional tomography scans after one shock (left), three shocks (middle) and nine shocks (right). Tests under high confinement. For a color version of the figure, see www.iste.co.uk/pijaudier/drystone.zip*

1.6.4. *Evolution of the pore size distribution*

On top of the development of cracking, the electrohydraulic shocks also affect the pore size distribution of the material. The above study has been complemented with additional measurements of the evolution of the pore size distribution of small specimens cored in the permeability specimens in order to determine whether there were any correlations. Mercury intrusion porosimetry has been used for this purpose. It is a routine technique with some drawbacks:

– It only characterizes the connected porosity which is accessible from the outer surface of the specimen. We do not intend, however, to consider the entire pore population, but rather the connected porous space that is at stake in the gas transfer process governing permeability. This drawback is therefore not important to us.

– The analysis is based on the assumption that pores are cylindrical with monotonically decreasing radius as mercury is injected into the specimen. The “ink bottle effect” [DIA 00]

may be important, i.e. small pores connected to large pores in the direction of the flow of mercury. This is avoided by performing several cycles of injection (upon cycles, mercury in such large pores remains trapped and is no longer accounted for in the calculation of pore size distribution).

– Finally, mercury intrusion porosimetry is destructive. For large pressures where small pores in the order of 10 nanometers or less become accessible, the issue of breakage of the pore walls may arise. This is the reason why the pore size distribution is restricted to the range between 20 and 30 nanometers and several micrometers.

The sample preparation consisted of coring, sawing and curing (24 h at 80°C) each specimen from larger specimens that had been subjected to electrical shock fracturing before and whose permeability had been already measured. Only specimens with high confinement corresponding to the data on permeability showed in Figure 1.6 are considered [KHA 15].

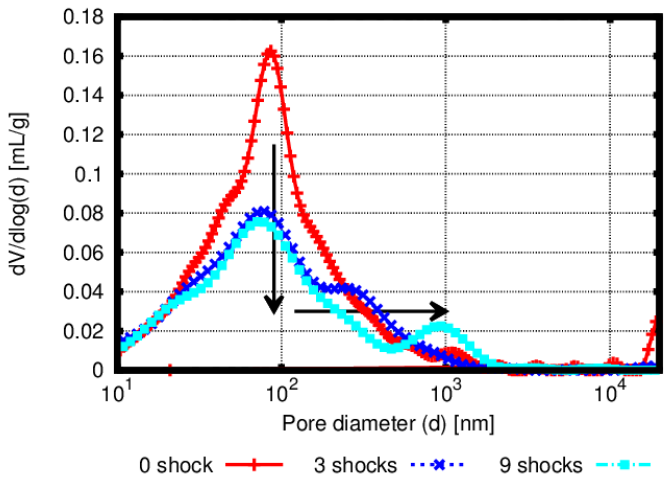

Figure 1.11. *Evolution of pore size distribution with the number of shocks. For a color version of the figure, see www.iste.co.uk/pijaudier/drystone.zip*

Three cylindrical samples for each specimen tested mechanically (8 mm in diameter and 10 mm in height) were prepared. The pore size distributions were further averaged. Figure 1.11 shows how the pore size distribution of the material evolved upon mechanical damage due to 0, 3 and 9 electrical shocks. The fraction of small pores (diameter of 100 nm) decreased, as did the fraction of larger pores (diameter of 500 nm). This effect was clearly related to the increase in permeability, on which large pores have a predominant influence.

1.7. Summary of the results on sandstone

Single shock tests were carried out under high confinement and with injected electrical energy of up to 14 kJ. The permeability of each specimen was measured before and after each test and is shown in Figure 1.12. Again, two distinct zones were observed. If the injected energy was below 4.2 kJ, no significant difference in permeability was observed. Then, the permeability increased almost linearly in a semi-log plot when the injected energy E_b increased from 4.2 to 14 kJ. This growth in permeability with injected electrical energy followed the same trend as for the mortar specimens.

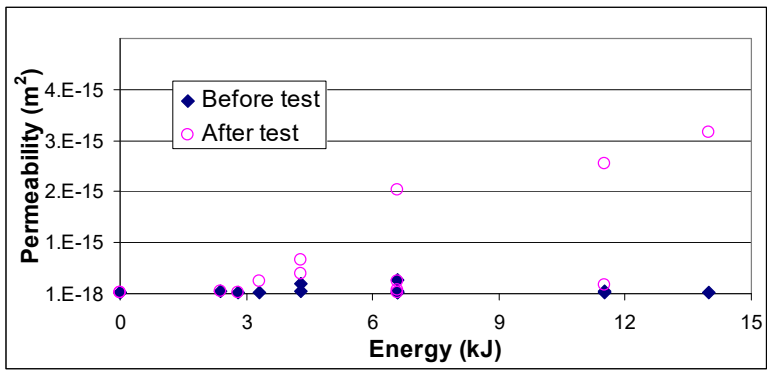

Figure 1.12. *Evolution of the permeability of sandstone specimens with injected energy before and after the shock test*

For the tests under repeated shocks, high confinement was also considered. The number of shocks varied from 2 to 8 (2, 3, 4, 5, 6 and 8 shocks) under a constant injected energy equal to 2.2 kJ. This energy corresponded to 80% of the energy injected at the onset of damage. The time delay between two shocks was long enough to avoid interaction between shock waves. The relative increase in the permeability of each specimen with the number of shocks is shown in Figure 1.12. If the number of shocks was less than 4, no significant changes were observed in the permeability. If the number of shocks was above 4, the relative variation in permeability increased almost linearly with number of shocks, which is the same as for the mortar specimens.

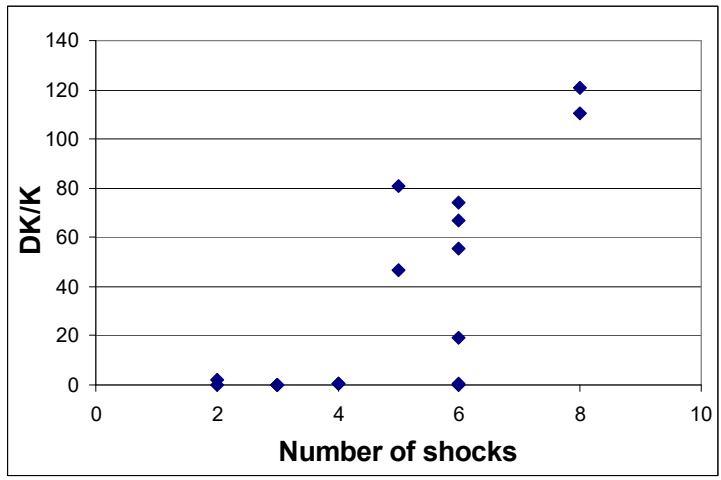

Figure 1.13. *Evolution of the ratio of the permeability of sandstone specimens with the number of shocks, under an injected energy equal to 2.2 kJ and high confinement*

1.8. Discussion

For both mortar and sandstone specimens, similar trends are observed. Above an energy threshold, test data on a single shock reveal a significant increase in permeability

whatever the confinement applied on the specimen. The fact that the load level should be increased in order to reach the fracture threshold with increasing confinement is a very classical result according to fracture mechanics analyses of hydraulic cracking [PAP 06, CHA 91].

As mentioned by Lopez and Jimeno [LOP 95], the pressure wave created by the blasting induces intense radial compression in the material, along with a tangent tensile stress. The radial fracturing of the specimen is obtained when the tangent stress exceeds the dynamic strength of the material. It is this radial fracturing which is at the origin of the increase in permeability. The experimental cracking patterns (vertical cracks), illustrated by X-ray scans, are in good agreement with existing numerical results in the literature [WAN 09].

The results obtained for repeated loads may also be compared with those obtained by Sanchidirian *et al.* [SAN 07] who measured an increase in damage of approximately 50% in rocks after 33 repeated blast rounds. Even if the damage created by a single shock cannot be measured in terms of permeability, the pore size distribution of the material should be affected by the loading. Note that there is also an endurance level below which microcracking never occurs, which is the same as in fatigue (see [CHK 09, BAZ 98]).

Finally, the increase in permeability due to microcracking is consistent with the data in the literature, e.g. on concrete specimens with a similar geometry [CHO 07]. This similarity is going to guide us in the development of theoretical models that should be able to provide a numerical simulation of the electrohydraulic fracture process.